Impacts of Shortwave Penetration Depth on Large-Scale Ocean Circulation and Heat Transport

COLM SWEENEY

Atmospheric and Ocean Sciences Program, Princeton University, Princeton, New Jersey

ANAND GNANADESIKAN, STEPHEN M. GRIFFIES, MATTHEW J. HARRISON, ANTHONY J. ROSATI, AND BONITA L. SAMUELS

NOAA Geophysical Fluid Dynamics Laboratory, Princeton, New Jersey

(Manuscript received 27 February 2004, in final form 15 September 2004)

ABSTRACT

The impact of changes in shortwave radiation penetration depth on the global ocean circulation and heat transport is studied using the GFDL Modular Ocean Model (MOM4) with two independent parameterizations that use ocean color to estimate the penetration depth of shortwave radiation. Ten to eighteen percent increases in the depth of 1% downwelling surface irradiance levels results in an increase in mixed layer depths of 3–20 m in the subtropical and tropical regions with no change at higher latitudes. While 1D models have predicted that sea surface temperatures at the equator would decrease with deeper penetration of solar irradiance, this study shows a warming, resulting in a 10% decrease in the required restoring heat flux needed to maintain climatological sea surface temperatures in the eastern equatorial Atlantic and Pacific Oceans. The decrease in the restoring heat flux is attributed to a slowdown in heat transport (5%) from the Tropics and an increase in the temperature of submixed layer waters being transported into the equatorial regions. Calculations were made using a simple relationship between mixed layer depth and meridional mass transport. When compared with model diagnostics, these calculations suggest that the slowdown in heat transport is primarily due to off-equatorial increases in mixed layer depths. At higher latitudes (5°–40°), higher restoring heat fluxes are needed to maintain sea surface temperatures because of deeper mixed layers and an increase in storage of heat below the mixed layer. This study offers a way to evaluate the changes in irradiance penetration depths in coupled ocean–atmosphere GCMs and the potential effect that large-scale changes in chlorophyll *a* concentrations will have on ocean circulation.

1. Introduction

Global ocean general circulation models (OGCMs) can treat solar heating of the ocean in terms of two processes. The first process is the heating due to infrared (IR) radiation, which is generally described as radiation above 700 nm. While IR radiation can represent 40%–60% (Mobley 1994) of the total downwelling surface ocean irradiance, it is almost completely (>99.9%) absorbed in the upper 2 m of the water column. The second process is the heating due to ultraviolet and visible wavelengths (VIS). VIS can penetrate much deeper than IR, and so its role in setting mixed layer depths (MLD) is far more important. The parameterization of ultraviolet and visible solar irradiance through the water column has taken on particular significance in recent climate modeling studies. This is because of the effects that it has on the mixed layer depths, overturning circulation, and the low-latitude sea surface temperatures of GCMs (Schneider and Zhu 1998; Murtugudde et al. 2002; Nakamoto et al. 2001; Rochford et al. 2002).

While many one-dimensional studies of the mixed layer have considered the importance of heating due to VIS at depth (i.e., Denman 1973; Simpson and Dickey 1981; Dickey and Simpson 1983; Lewis et al. 1983; Woods and Onken 1982; Woods et al. 1984; Martin 1985; Siegel et al. 1999, 1995; Ohlmann et al. 1996, 1998), the climate modeling community has been slow to implement these parameterizations in OGCMs. As a first step, most models assume that all of the solar irradiance is absorbed at the surface in the same way that latent and sensible heat are passed across the air–sea interface. In an effort to provide a more realistic parameterization, many OGCMs (i.e., Rosati and Miyakoda 1988) use two exponential functions whose *e*-folding depths provide parameterization of both IR

Corresponding author address: Colm Sweeney, AOS Program, 302 Sayre Hall, P.O. Box CN710, Princeton, NJ 08544-0710.
E-mail: csweeney@splash.princeton.edu

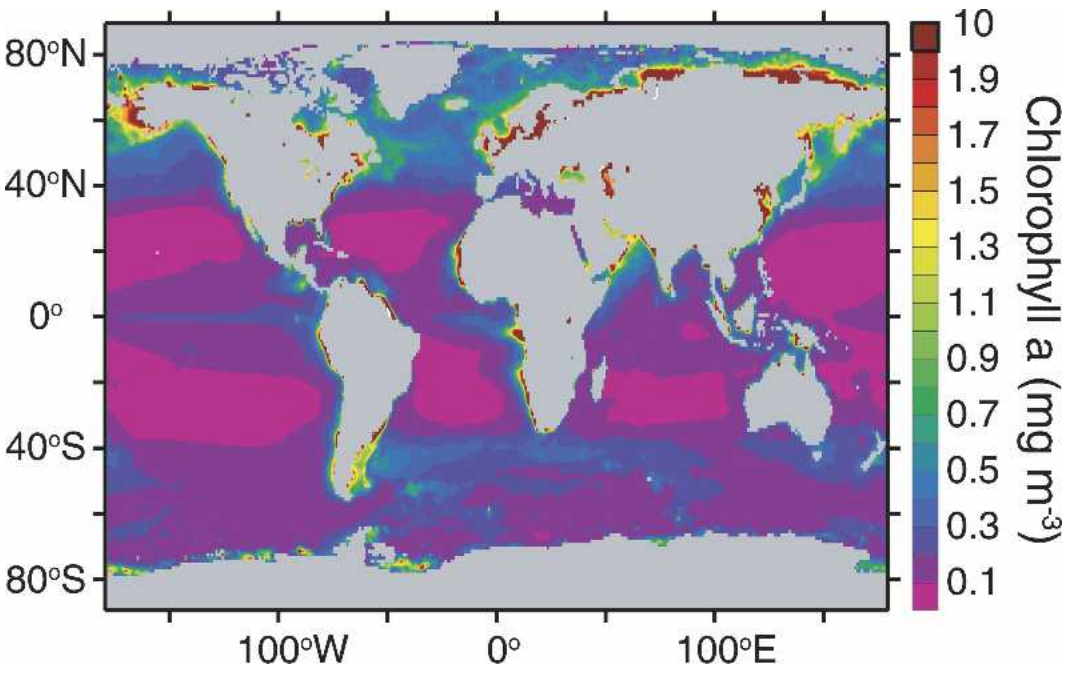

FIG. 1. Mean annual chlorophyll *a* (mg m^{-3}) climatology produced from 8-day composites of SeaWiFS images taken from 1999 to the end of 2001 (Yoder and Kennelly 2003; see online at http://www.po.gso.uri.edu/~maureen/sm_seawifs.html). High primary productivity in the eastern equatorial, near-shore, and upwelling zones leads to high concentrations of chlorophyll a in these areas while low productivity in the subtropical gyres leads to low concentrations of chlorophyll *a*.

and VIS (Paulson and Simpson 1977). The double exponential parameterization expands on the single exponential function used by Denman (1973). While Paulson and Simpson (1977) specify six different water types described by Jerlov (1968), climate models have generally incorporated only a single water type that best represents the mean water type of the open ocean. A more recent parameterization of solar irradiance penetration in the water column using remotely sensed observations of chlorophyll *a* (Morel 1988; Morel and Antoine 1994; Ohlmann 2003) and availability of ocean color satellite data [i.e., Coastal Zone Color Scanner (CZCS), Sea-Viewing Wide-Field-of-View Sensor (SeaWiFS), and Moderate-Resolution Spectroradiometer (MODIS)] has led to several studies exploring the benefit of the added spatial and temporal variation in shortwave penetration depth. These studies show the importance of considering both spatial (Murtugudde et al. 2002) and seasonal (Nakamoto et al. 2001; Rochford et al. 2002) variability of solar irradiance penetration due to changes in chlorophyll *a* concentrations in the surface waters.

In particular, studies in the central equatorial Pacific Ocean have suggested that chlorophyll *a* may have significant impact on sea surface temperatures. Chlorophyll *a* concentrations in this region have been observed to vary by up to a factor of 20 during recent El Niño–La Niño events (Strutton and Chavez 2004). Similarly, large changes in the chlorophyll *a* concentration in the western equatorial Pacific have been observed during westerly wind bursts, which increase surface heating in the mixed layer by as much as 0.13°C $month^{-1}$ (Siegel et al. 1995). This has special significance in the western equatorial Pacific region because of the sensitivity of the lower tropospheric convection cell strength to the heat content of western warm pool (Gildor et al. 2003; Siegel et al. 1995).

In addition to temporal variability, there also exists a large zonal gradient in surface chlorophyll *a* (Fig. 1) in the equatorial Pacific and Atlantic Oceans. Many investigators have speculated that the neglect of the resulting gradients in shortwave absorption could account for some of the cold bias seen in coupled ocean–atmospheric GCMs within the cold tongue region. However, Nakamoto et al. (2001) showed quite the opposite trend when they compared the constant attenuation depth model (23 m) with the chlorophyll *a* concentration dependent parameterization of Morel and Antoine (1994). In areas of the eastern equatorial Pacific where the attenuation of solar irradiance was more pronounced because of high chlorophyll *a* concentrations, lower SSTs were found. They attribute the decrease in SSTs to an increase in the strength of the equatorial undercurrent triggered by the decrease in equatorial mixed layer depths. In a similar experiment, Murtugudde et al. (2002) compared a chlorophyll *a*–dependent parameterization with a constant attenuation of solar irradiance (25 m) and found no change in temperatures at

the equator but a net increase in diverging surface currents.

The objective of this study is to lay out how changes in the parameterization of solar irradiance or actual chlorophyll *a* concentrations will affect mixed layer depths, meridional overturning circulation, and sea surface temperatures (SSTs) in GCMs. We have chosen to do this study using an ocean-only GCM that restores SSTs to climatological values instead of a coupled ocean–atmosphere GCM where feedback processes between ocean and atmosphere may obscure the direct effect of solar penetration to the ocean. While other studies (Schneider and Zhu 1998; Murtugudde et al. 2002; Nakamoto et al. 2001; Rochford et al. 2002) have chosen to compare very different parameterizations, this study has been specifically designed to compare two parameterizations that are very similar. They are similar because they both incorporate the same chlorophyll *a* climatology. The subtle difference between the parameterizations used in this study provides a realistic sensitivity test making it possible to quantify how GCMs can be affected by different solar irradiance parameterizations and observed chlorophyll *a* concentrations.

2. Method

a. The circulation model

Both optical models were tested using the most recent version of the National Oceanic and Atmospheric Administration (NOAA) Geophysical Fluid Dynamics Laboratory (GFDL) Modular Ocean Model (MOM4: Griffies et al. 2003), which solves the hydrostatic, z-coordinate primitive equations. The model resolution is 2° in the east–west direction. The north–south resolution varies from 2° in midlatitudes, to ⅔° in the Tropics. Enhanced resolution is also used in the Arctic, where the tripolar grid of Murray (1996) is used, with an average resolution of 2° × 1°. The model has 50 vertical levels. In the top 230 m the resolution is uniform with a grid spacing of 10 m. Below 230 m vertical grid spacing increases linearly to 366 m at the bottommost tracer cell.

The model is initialized using temperatures and salinities from the NOAA *World Ocean Atlas* (see online at http://www.nodc.noaa.gov) and run for a 10-yr period. In the model experiments, both temperature and salinity are restored to seasonally varying observations over a 10-day period. Additional fluxes of heat and freshwater are taken from the output of the GFDL atmospheric model run according to the Atmospheric Model Intercomparison Project (AMIP) protocol. Wind stress is given from a reanalysis dataset created for the Ocean Model Intercomparison Project (OMIP) (Roeske 2001), which includes realistic levels of synoptic variability. For the mixed layer the *K*-profile parameterization (KPP) scheme of Large et al. (1994) is employed. For the vertical and horizontal advection the "quicker" scheme of (Holland et al. 1998; Pacanowski and Griffies 1999) is employed. The neutral diffusion (Redi 1982) and thickness diffusion (Gent et al. 1995) according to Griffies (1998) and Griffies et al. (1998) is used with an along-isopycnal diffusivity of 1000 $m^2\ s^{-1}$ for both tracers and layer thickness. Lateral friction is parameterized using a Laplacian viscosity. This consists of two components: one given by a background value that is constant in time and equivalent to the grid spacing times a velocity scale and an additional Smagorinsky-type viscosity that depends on the local horizontal shears (Griffies and Hallberg 2000; Smagorinsky 1963). Away from the equator a dimensionless constant of 2 is used to define the value of Smagorinsky component and a velocity scale of 0.5 $m\ s^{-1}$ is used to set the constant term. At the equator the velocity scale used to set the viscosity was much lower (0.05 $m\ s^{-1}$) and the Smagorinsky term was set to zero. This allows for a realistically narrow equatorial undercurrent and the presence of tropical instability waves. Vertical diffusivity was made a function of depth using the vertical profile of Bryan and Lewis (1979) with values of 0.05 $cm^2\ s^{-1}$ in the surface ocean and 1.05 $cm^2\ s^{-1}$ in the deep ocean.

b. Formulation of shortwave penetration

Solar penetration shifts the location of solar shortwave heating downward in the ocean column, resulting in heating at depth. The profile of downward radiative heat flux $I(x, y, z)$ is represented as

$$I(x, y, z) = I_{o-}(x, y)J(z), \tag{1}$$

where I_{o-} (W m^{-2}) is the total shortwave downwelling radiative flux per unit area incident just below the sea surface and $J(z)$ is a dimensionless attenuation function that ranges from 1 at the surface to an exponentially small value at depth. Note that the total downwelling radiation I_{o-} is to be distinguished from the total shortwave flux I_o, where $I_{o-} = (1 - \alpha)I_o$, with $\alpha \approx 0.06$ being the sea surface albedo (Morel and Antoine 1994).

Shortwave heating affects the local temperature $(T)_t$ in a Boussineq fluid according to

$$(T)_t = -(1/\rho C_p)\partial/\partial z(\rho C_p F^z - I). \tag{2}$$

In this equation, F^z accounts for vertical processes such as advection and diffusion and C_p is the heat capacity of seawater. Shortwave heating leads to the following net heating rate (K $m\ s^{-1}$) over a column of ocean fluid

$$(1/\rho C_p)\int_{-H}^{\eta} dz\,\partial_z I = (1/\rho C_p)[I(\eta) - I(-H)], \tag{3}$$

with $I(\eta)$ as the solar radiation at the free surface ($z = \eta$).

To compare the effect of solar irradiance parameterization on the ocean general circulation, two parameterizations have been picked that have been explicitly developed for large-scale ocean models with low resolution in depth space ($\Delta z > 5$ m).

1) MOREL AND ANTOINE SOLAR IRRADIANCE PARAMETERIZATION

Morel and Antoine (1994, hereinafter MA94) expand the exponential function used by Denman (1973) into three exponentials to describe solar penetration into the water column. The first exponential is for wavelengths > 750 nm (i.e., I_{IR}) and assumes a single attenuation of $0.267 \cos\theta$ m, where θ is the solar zenith angle. For simplicity, we assume that the solar zenith is zero throughout the daily integration of the model. Thus, the resulting equation for the infrared portion of the downwelling radiation is

$$I_{\mathrm{IR}}(x, y, z) = I_{\mathrm{IR}-}(x, y)e^{(-z/0.267\cos\theta)}, \tag{4}$$

where z is the depth in meters and $I_{\mathrm{IR}-}(x, y)$ is a fraction, of the total downwelling radiation I_{o-} such that

$$I_{\mathrm{IR}-}(x, y) = J_{\mathrm{IR}}I_{o-}, \tag{5}$$

where J_{IR} is the fraction solar radiation in the infrared (750–2500 nm) band. Although MA94 note that water vapor, zenith angle, and aerosol content can each affect the fraction of incoming radiation that is represented by infrared and visible light, in the present implementation, we have chosen to keep these fractions constant so that $J_{\mathrm{IR}} = 0.43$. For the models used in this paper, the top level is 10 m thick so that essentially all infrared energy is absorbed in the top layer.

The second and third exponentials represent a parameterization of the attenuation function for downwelling radiation in the visible range (300–750 nm) in the following form:

$$I_{\mathrm{VIS}}(x, y, z) = I_{\mathrm{VIS}\text{-}}(x, y)[V_1e^{(-z/s1)} + V_2e^{(-z/s2)}]. \tag{6}$$

This form further partitions the visible radiation into long (V_1) and short (V_2) wavelengths, assuming

$$F_{\mathrm{IR}} + F_{\mathrm{VIS}} = 1 \tag{7}$$

and

$$V_1 + V_2 = 1; \tag{8}$$

V_1, V_2, ζ_1, and ζ_2 are calculated from an empirical relationship as a function of chlorophyll *a* concentration using methods from MA94 (our appendix A). Throughout most of the ocean, $V_1 < 0.5$ and $V_2 > 0.5$. The *e*-folding length scales ζ_1 and ζ_2 are the *e*-folding depths of the long (ζ_1) and short visible and ultraviolet (ζ_2) wavelengths. Based on the chlorophyll *a* climatology used in the GFDL model, ζ_1 should not exceed 3 m while ζ_2 will vary between 30 m in oligotrophic waters and 4 m in coastal regions. All of these constants are based on satellite estimates of chlorophyll *a* plus pheaophytin-*a*, as well as parameterizations that have "nonuniform pigment profiles" (MA94). The nonuniform pigment profiles have been proposed to account for deep chlorophyll maxima that are often observed in highly stratified oligotrophic waters (Morel and Berthon 1989).

2) THE OHLMANN (2003) SHORTWAVE PENETRATION MODEL

The second light transmission parameterization that we use to compare with that of MA94 is based on work done by Ohlmann (2003, hereinafter O03). Instead of three exponentials this parameterization uses two exponential functions, which broadly describe the attenuation of downwelling solar radiation in the visible and infrared wavebands. The HYDROLIGHT in-water radiative transfer model that resolves wavelengths from 250 to 2500 nm (Ohlmann and Siegel 2000) was used to produce synthetic data that could be used to fit a two exponential function and a term that takes into account the incident angle (θ) of the sun and the cloud index (ci):

$$I(x, y, z) = I_{o-}(x, y)[V_1e^{(-z/s1)} + V_2e^{(-z/s2)}] \times [1 + H(\theta)G(\mathrm{ci})]. \tag{9}$$

The first exponential parameters (V_1 and ζ_1) are used to describe the UV–visible spectrum (300–750 nm). It is this exponential that describes light transmission below 8 m. The second exponential parameters (V_2 and ζ_2) represent the fraction of light in the infrared spectrum (750–2500 nm) and attenuation depth of light between 2 and 8 m. Above 2 m a more rigorous model is needed to look at skin temperature and boundary layer dynamics (Ohlmann and Siegel 2000). All of the parameters in Eq. (9) have been fit as a logarithmic or exponential functions of chlorophyll using a full spectrum (300–2500 nm) light model called HYDROLIGHT (our appendix B). From the HYDROLIGHT model it can be observed that the solar angle of incidence significantly effects the solar transmission when the angle of incidence is $>60°$. Below that value the angle of incidence is not considered to significantly affect the transmission of light (O03). For consistency we have kept the angle incidence and cloud index equal to 0 in our implementation of this parameterization.

3) SEAWIFS-BASED CHLOROPHYLL *a* CLIMATOLOGY

A chlorophyll *a* climatology was produced from estimates of surface chlorophyll *a* using SeaWiFS. The climatology is based on 8-day composites of SeaWiFS images taken from 1998 through 2001. The climatology calculates the median chlorophyll *a* concentration on the 15th day of each month considering all data 15 days

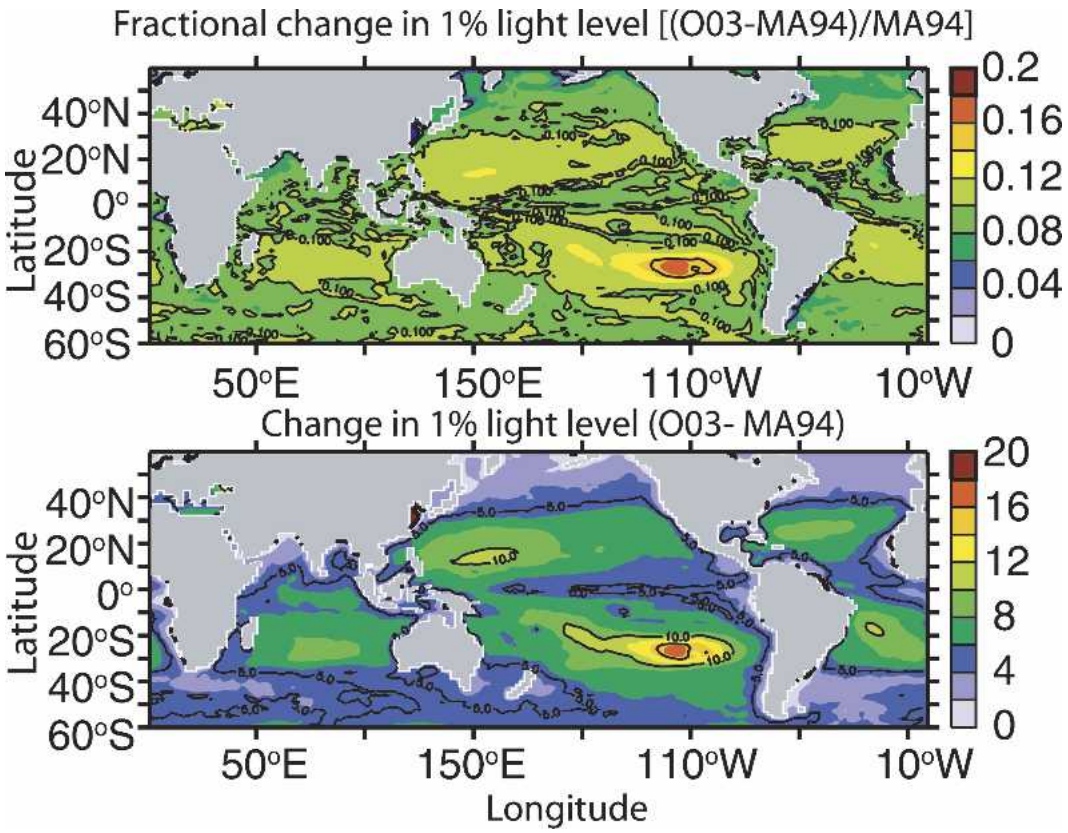

FIG. 2. (top) Fractional change in depth of 1% light level. (bottom) Change in depth (m) of 1% light level. Throughout most of the world oceans the Ohlmann (2003) parameterization predicts that the 1% light level is about 10% deeper than that of Morel and Antoine (1994). The fractional difference in the 1% light level increases in low chlorophyll *a* areas like the subtropical gyres. By contrast, the difference decreases in higher chlorophyll *a* areas such as the eastern equatorial Pacific region.

before and 15 days after the 15th day of each month. This dataset is available from the GFDL NOAA Operational Model Archive and Distribution System (NOMADS) server where MOM4 datasets are distributed (find online at http://nomads.gfdl.noaa.gov/).

3. Results

a. Shortwave penetration depths differences between MA94 and O03

As expected, the same spatial patterns exist for both light transmission parameterizations because both parameterizations use the same satellite observations of ocean color (Fig. 1). The main difference between the O03 and MA94 light transmission parameterizations is the penetration depth. Throughout most of the world oceans, the O03 parameterization predicts that the 1% light level is about 10% deeper than that of MA94 (Fig. 2). The difference in penetration depth between the two parameterizations also increases as chlorophyll *a* decreases (the largest differences are found in clear water). This difference is highlighted in the low chlorophyll *a* (0.045 mg m^{-3}) area in the subtropical gyre of the South Pacific where there is more than an 18% difference in the depth of the 1% light levels. By contrast, in the high chlorophyll *a* (0.24 mg m^{-3}) eastern equatorial Pacific region the difference between penetration depths is less than 10%.

The potential impact of the differences in penetration depth in O03 and MA94 can be further illustrated by looking at the fraction of downwelling shortwave radiation that is absorbed over a 10-m slab centered at the average depth of the annual mixed layer (Table 1). For the eastern equatorial Pacific the O03 parameterization increases shortwave heating at the top of the mean annual thermocline by ~48% relative to MA94. In the southern subtropical gyre region the increase in shortwave heating at the top of the mean annual thermocline is ~58%.

b. Model derived differences

While the differences in the penetration depth between O03 and MA94 are intriguing, the purpose of this study is not to analyze these differences in pa-

TABLE 1. The potential monthly change in temperature due to shortwave radiation over a 10-m slab centered on the average annual mixed layer depths (Schneider and Zhu 1998) of the eastern equatorial (2°S–2°N and 120°–160°W) and subtropical gyre (28°–20°S and 90°–110°W) regions of the Pacific Ocean. This calculation does not account for any mixing or diffusion of heat.

	Eastern equatorial Pacific		Southern subtropical Pacific	
	Morel and Antoine	Ohlmann	Morel and Antoine	Ohlmann
Observed avg mixed layer depth (m)	36	36	69	69
Calculated 1% transmission depth (m)	50	55	89	101
Observed net SW radiation (W m^{-2})	257	257	199	199
Calculated net heating at MLD (°C $month^{-1}$)	0.32	0.47	0.13	0.21

rameterizations but to understand the effects that these differences in shortwave penetration will have on the ocean circulation. From this perspective we focus on model diagnostics in the low latitude regions of the Pacific where the apparent differences between O03 and MA94 shortwave penetration profiles, and the resulting changes in circulation, are most pronounced.

1) CHANGES IN MIXED LAYER DEPTH

As expected, the most pronounced difference between the model run with the O03 and the model run with the MA94 parameterization are changes in the mixed layer depth (Fig. 3). These changes range from values of <3 m at the equator to values of up to 20 m in the subtropical gyres. At latitudes greater than 40° no significant change in mixed layer depth is observed. A meridional view of the average change in temperature in the upper 200 m illustrates that although this model restores sea surface temperatures to climatological values, there are significant changes in the temperature at the base of the mixed layer >0.5°C (Fig. 4). Large changes in the mixed layer depth coincide with large changes in temperature at the base of the mixed layer. As noted in the difference in light penetration depth, the O03 model run shows significant increases in mean annual temperature at the base of the mixed layer in addition to large changes in mixed layer depth in the subtropical gyre areas where there is less chlorophyll *a*.

2) RESTORING HEAT FLUXES

In a one-dimensional ocean model without any restoring heat flux, deeper mixed layers would presumably lead to entrainment of deeper and colder waters from below, reducing surface temperature and increasing temperatures at the base of the mixed layer. From this perspective, the large air–sea flux of heat needed to maintain climatological sea surface temperatures at the equator (~100 W m^{-2}) would increase with an increase in mixed layer depth. In our GCM comparison, we see the opposite trend (Fig. 5). The model using the O03 parameterization, which has deeper mixed layer depths both on and off the equator, actually requires less restoring heat flux (10 W m^{-2}) to maintain climatological sea surface temperatures at the equator (implying that the surface temperatures have warmed). This trend can be found in both the Atlantic and Pacific basins. In the equatorial Pacific, the difference between the two model runs is greatest to the east, which coincides with much warmer waters below the mixed layer (Fig. 6) using the O03 parameterization.

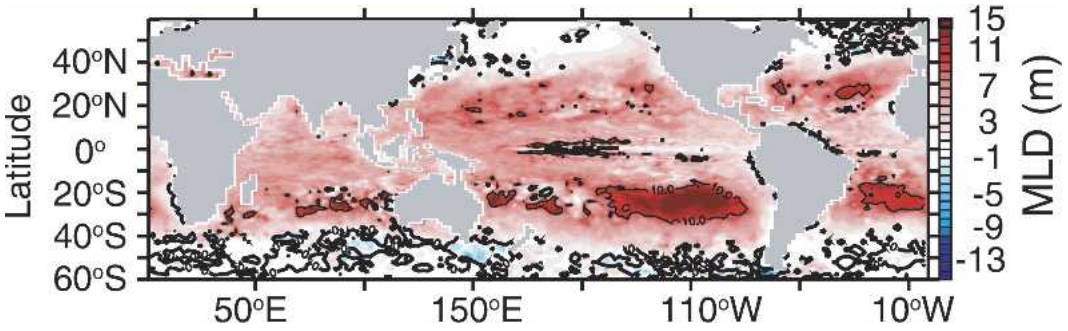

FIG. 3. Difference in mixed layer depth (m) using parameterization of Morel and Antoine (1994) and Ohlmann (2003). Mixed layers are calculated as the depth at which the density of seawater is 0.030 kg m^{-3} greater than surface values. As with the penetration depth (Fig. 2), greatest increases in mixed layer depth are observed in low chlorophyll *a* areas like the subtropical gyres. The difference between the parameterization of Morel and Antoine (1994) and Ohlmann (2003) decreases in higher chlorophyll *a* areas such as the eastern equatorial Pacific region.

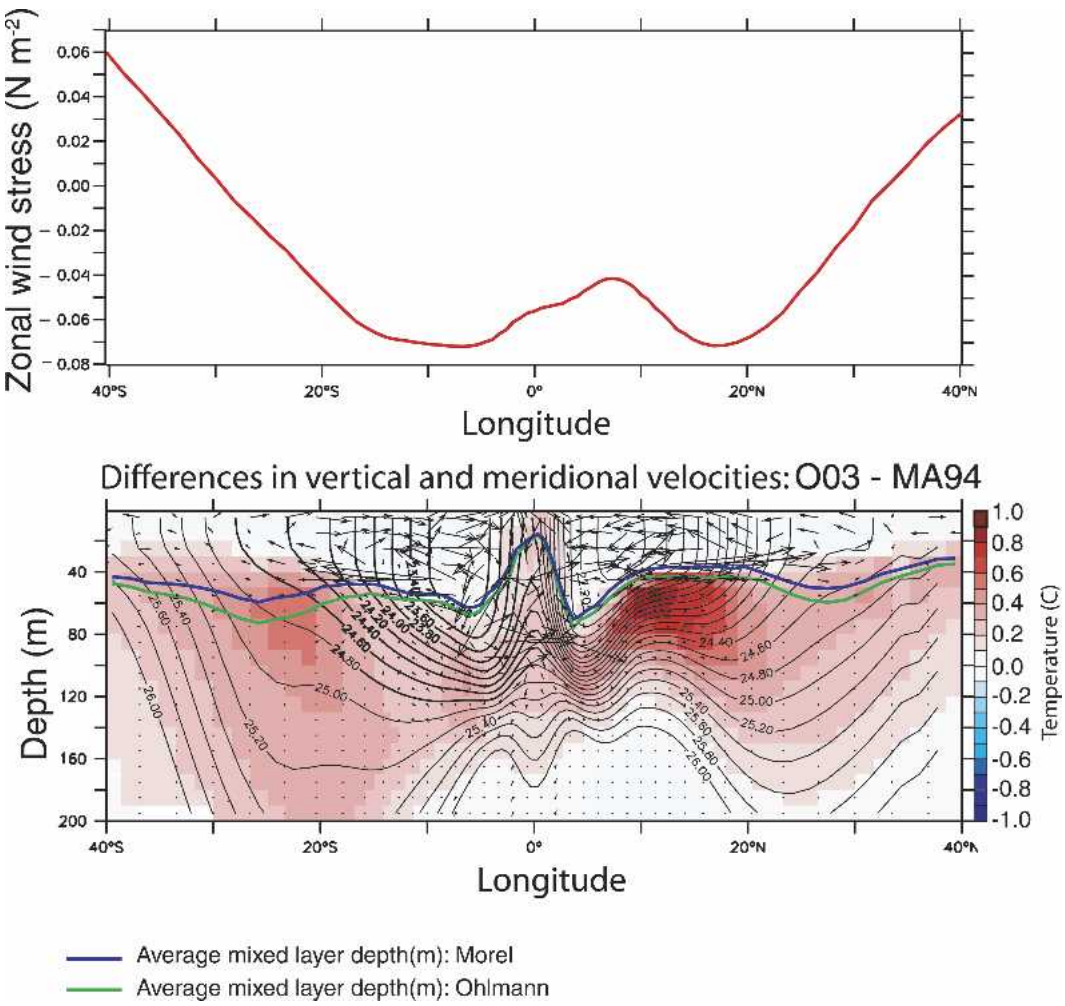

FIG. 4. (top) Average zonal wind stress (+ eastward, − westward) in the Pacific basin. (bottom) Contour lines show σ_τ for MA94 line, and color indicates magnitude of temperature difference between O03 and MA94. Vector arrows signify difference in average vertical and meridional flow. Blue line indicates the average mixed layer depth for MA94, and the green line indicates the average mixed layer depth for O03. Weak stratification and low wind speeds in the subtropical gyres are primarily responsible for the large change in mixed layer depths observed between model runs using O03 and MA94 shortwave parameterizations.

Five degrees north and south of the equator, the restoring heat fluxes of the O03 parameterized model run become greater than those of the MA94 parameterized model run, as one might expect with deeper mixed layers in a 1D column. The increase in restoring heat fluxes needed to maintain climatological SSTs for the O03 parameterized model run reaches a maximum at 20°N and 20°S in locations coincident with maximums in light penetration, mixed layer deepening, and submixed layer temperature changes (Figs. 4 and 5).

3) MERIDIONAL CHANGES IN CIRCULATION AND HEAT TRANSPORT

As can be inferred from the observations of changes in the restoring heat flux, the O03 parameterization run is not as effective at transporting heat to the higher latitudes as the MA94 parameterization run. The difference in the mean meridional heat transport between the O03 parameterization and MA94 parameterization reaches values as high as 0.08 PW 7° north and south of the equator (Fig. 7: <4% of the total meridional overturning circulation at the equator). In the Pacific, this decrease in heat transport is most likely the result of a slowdown in the meridional overturning circulation of almost 3 Sv (Sv $\equiv 10^6$ m^3 s^{-1}) between the equator and 15°N and 15°S (Fig. 8).

Figure 4 shows that using the O03 parameterization resulted in a slowdown of meridional transport of water to higher latitudes at the surface and an increase in the meridional transport to higher latitudes at the depths of the mixed layer.

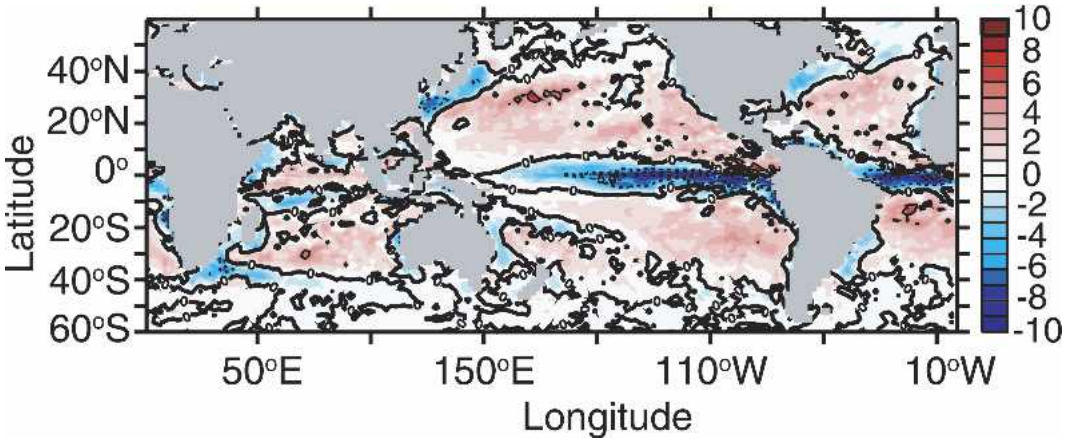

FIG. 5. Difference in restoring heat flux (W m^{-2}) as a result of different parameterization of penetrating solar irradiance: Ohlmann (2003) minus Morel and Antoine (1994). The change in restoring heat fluxes in the eastern equator (-10 W m^{-2}) represent a 10% decrease in the heat needed to maintain sea surface temperatures at climatological values. One-dimensional models would predict an increase instead of a decrease in the restoring heat flux with increased penetration of shortwave irradiance at the equator. The change in restoring heat fluxes in the subtropical gyre regions ($\sim$4 W m^{-2}) represents an increase of almost 20%.

4. Discussion

a. Changes in mixed layer depth

From the results described above, the increase in shortwave irradiance at depth associated with the O03 parameterization over most of the low-latitude oceans, caused an increase in mixed layer depth. It is also clear that the difference between the O03 and MA94 parameterizations increases with decreases in the chlorophll *a* concentrations. It is not clear, however, that there is a direct relationship between the increase in penetration depth and the increase in mixed layer depth. Instead, there is a combination of likely causes for changes in mixed layer depths between parameterizations. These include density gradient below the mixed layer, wind speeds, and relative depth of the mixed layer.

In a one-dimensional analysis Strutton and Chavez (2004) point out that the relatively shallow mixed layer depths of the eastern equatorial Pacific make the mixed layer heat budget of this region particularly susceptible to changes in chlorophyll *a* concentrations. They point out that for mixed layer depths of 10 m the monthly heating rate would more than double as a result of a change in chlorophyll *a* concentrations from 0.1 to 0.4 mg m^{-3}. One would also expect the same sensitivity from a model with a change in parameterization of shortwave penetration.

Results from the eastern equatorial region show quite the opposite. The change in penetration depth has significantly less effect on the mixed layer depths in the eastern equatorial Pacific than it does in areas to the west or at higher latitudes. There are three possible reasons for this behavior. First, most of the heat is absorbed in the top layer of the model with high concentrations of chlorophyll *a*. Thus, small changes in penetration of solar irradiance make little difference in such regions. Second, it is likely that large density gradients below the mixed layer (Fig. 4) and the overwhelming effect of the high zonal winds are the main factors that determine variability of the mixed layer depth in the eastern equatorial Pacific. Third, Table 1 indicates that the net change in heating at the base of the mixed layer is less in the equatorial region than areas with lower chlorophyll *a* concentrations.

In contrast, the biologically unproductive area of the subtropical gyre regions show large changes in mixed layer depths. There are three compounding factors driving these large changes in mixed layer depth: 1) low wind speeds over these regions, 2) small density gradient at the top of the thermocline, and 3) significantly more light penetration at depth in an area of low chlorophyll *a* concentrations. While regions just off the equator have much lower concentrations of chlorophyll *a*, a high wind regime (Fig. 9a) maintains deep mixed layer depths. Thus, small changes in the parameterization of chlorophyll *a* have little effect on the mixed layer depth in regions with strong winds. These observed relationships have been shown in one-dimensional models (Denman, 1973; Simpson and Dickey 1981), which have tested the effect of different parameterizations of solar irradiance on the mixed layer depth. While parameterizations of solar irradiance can have significant effects on mixed layer depths at low wind speeds, little difference in the mixed layer depth is seen at high winds (>8 m s^{-1}). In most studies, 1D models have shown that at higher wind speeds the mixed layer depends equally on the turbulent energy produced by the wind stress and the density gradient below the mixed layer (a measure of the buoyancy force encountered by the wind-driven turbulent mix-

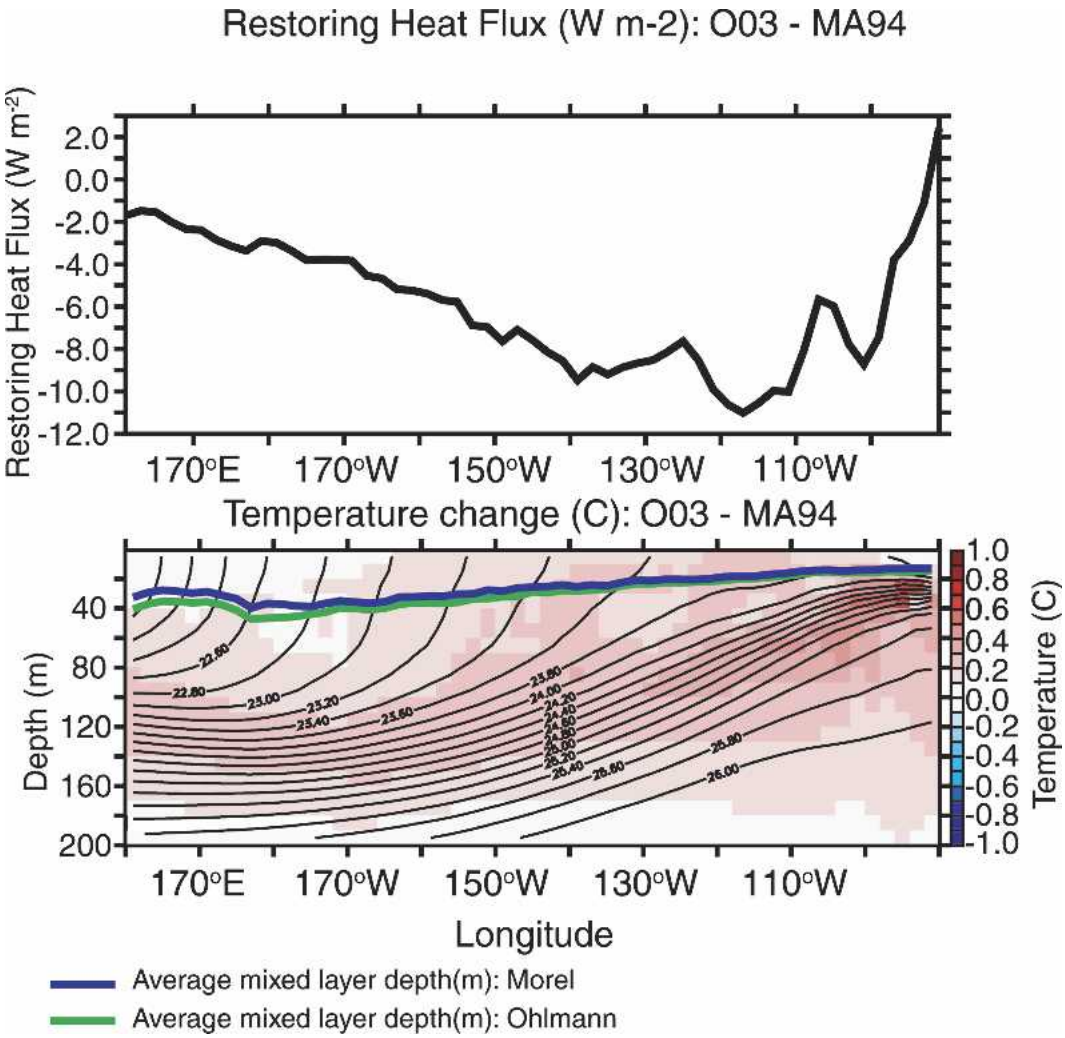

FIG. 6. (top) Difference in restoring heat flux (W m^{-2}) as a result of different parameterization of penetrating solar irradiance average over one annual cycle from 5°S to 5°N. (bottom) Contour lines show σ_τ for MA94 line, and color indicates magnitude of temperature difference between O03 and MA94. Blue line indicates the average mixed layer depth for MA94, and the green line indicates the average mixed layer depth for O03. The large decreases (10%) in the restoring heat needed with increased penetration of solar irradiance in the eastern equatorial Pacific counters one-dimensional modeling results that would have predicted a decrease in SST. Mixed layer depths are defined in each model as the depth at which the density is 0.03 kg m^{-3} greater than the surface density.

ing). Lewis et al. (1983) also uses similar one-dimensional models to argue that the mixed layer depths in optically clear waters of the subtropical gyres are likely to respond to changes in chlorophyll *a* concentrations. They argue that subsurface maximum in chlorophyll *a* are the primary driver for "nonuniform" changes in the local heating rates down through the water column. While there is no doubt that this may be a factor in the real ocean, neither the O03 nor MA94 parameterization simulate the nonuniformities in subsurface irradiance absorption to the degree needed to provide deeper mixed layers suggested by Lewis et al. (1983).

From the preceding discussion it is easy to understand why we see little change in the mixed layer at high latitudes. Essentially there are three basic reasons for this result. The first is high winds, which leads to the second—deeper mixed layer depths at high latitudes. The final reason is that the absolute value of downwelling shortwave irradiance at the sea surface is low. In summary, very little shortwave radiation makes it below the existing mixed layer depths no matter what the chlorophyll *a* concentration is at high latitudes.

b. Changes in circulation and restoring heat fluxes

While the one-dimensional effects of different parameterizations of solar irradiance in the water column are primarily manifested in changes in predicted mixed layer depth (Denman 1973; Simpson and Dickey 1981; Dickey and Simpson 1983; Woods and Onken 1982;

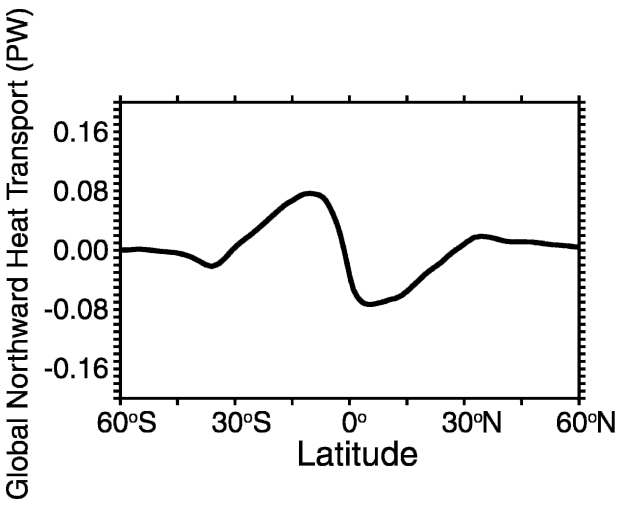

FIG. 7. Change in global heat transport (PW) as a result of a change in the parameterization of solar irradiance through the water column (O03 − MA94). The result of the slowdown in the surface water velocity caused by using the O03 parameterization (relative to the MA94 parameterization) is small (4%) for net meridional heat transport.

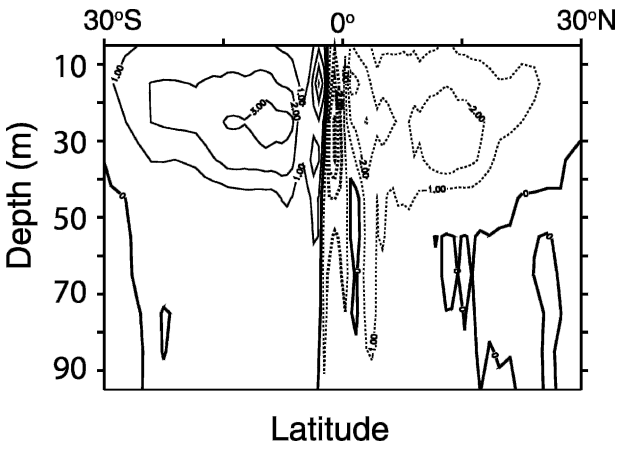

FIG. 8. Difference in the meridional overturning (Sv) from 30°S to 30°N in the Indian and Pacific Ocean basins due to a change in parameterization of solar irradiance throughout the water column (O03 − MA94).

Siegel et al. 1995; Ohlmann et al. 1996), this three-dimensional (GCM) study illustrates secondary responses to changes in the mixed layer depth. The changes in mixed layer depth appear to significantly affect surface restoring heat fluxes and, to a lesser degree, meridional heat transport in the Tropics. The large-scale meridional transport of water from the equatorial Pacific to the midlatitudes is primarily driven by easterly winds (τ_x/ρ). In addition to forcing surface waters away from the equator, easterly winds also drive warm, less dense waters to the west. The resulting pressure gradient forces an opposing meridional transport pushing waters to the low latitudes. The resulting meridional transport (M_y) can be quantified as

$$\int_{D_{\mathrm{ML}}}^{\eta} -\frac{1}{\rho_o}\frac{\partial p}{\partial x}\,dz + \frac{\tau_x}{\rho_o} = fM_Y, \tag{10}$$

where $(1/\rho_o)\partial p/\partial x$ is the zonal pressure gradient, f is Coriolis force, η is the sea surface height, and D_{ML} is the mixed layer depth. The magnitude of the two components driving meridional transport in Eq. (10) are illustrated in Fig. 9. The first is the Ekman component, τ_x/ρ, which is considered to be constant in both model runs. The second is the geostrophic component, $\int_{D_{\mathrm{ML}}}^{\eta} -(1/\rho)(\partial p/\partial x)dz$, which is calculated to be significantly different for each experiment at 5°S in the equatorial Pacific. Figure 10 suggests that there is very little difference between the zonal pressure gradient, indicating that mixed layer depths are the primary cause of the differences in the total mixed layer meridional transport (fM_y) between these two models. The difference between the fM_y using the O03 and MA94 parameterizations is compared directly with the model diagnostics at 5°S in the equatorial Pacific (Fig. 11). Although small-scale differences exist because of lateral viscosity and other small-scale processes, the large-scale similarity between model simulated meridional transport and that computed [Eq. (10)] suggest that mixed layer depths are a dominant source of the variability in meridional mass flux at 5°S.

While it is clear from Eq. (10) that changes in either the zonal pressure gradient or the mixed layer depth, changing the shortwave penetration apparently results in a change in the mixed layer depth, without major changes in the baroclinic structure and thus in the surface pressure gradient. Deepening mixed layers throughout the tropical oceans results in an ~10% decrease in poleward transport of water in the surface oceans using the O03 parameterization (relative to the MA94 parameterization).

Interestingly, the slowdown in poleward transport of surface waters results in a much smaller (4%) change for the net meridional heat transport (Fig. 7). We attribute the small decrease in heat transport despite the larger changes in mass transport to changes in the temperature gradients in mixed layer off the equator. A moderate (10%) decrease in the surface restoring heat flux (Fig. 5) at the equator indicates a warming of surface waters at the equator. At the same time, a more pronounced (>20%) increase in restoring heat flux off the equator in the subtropical gyre areas indicates a cooling of surface waters. The combination of these results is a significant increase in the meridional heat gradients that significantly impacts the total poleward heat transport.

To further test the effect of changing mixed layer depths on the overturning circulation and heat transport, a third model run was performed that combined both the O03 and MA94 shortwave parameterizations. The MA94 solar irradiance parameterization was used

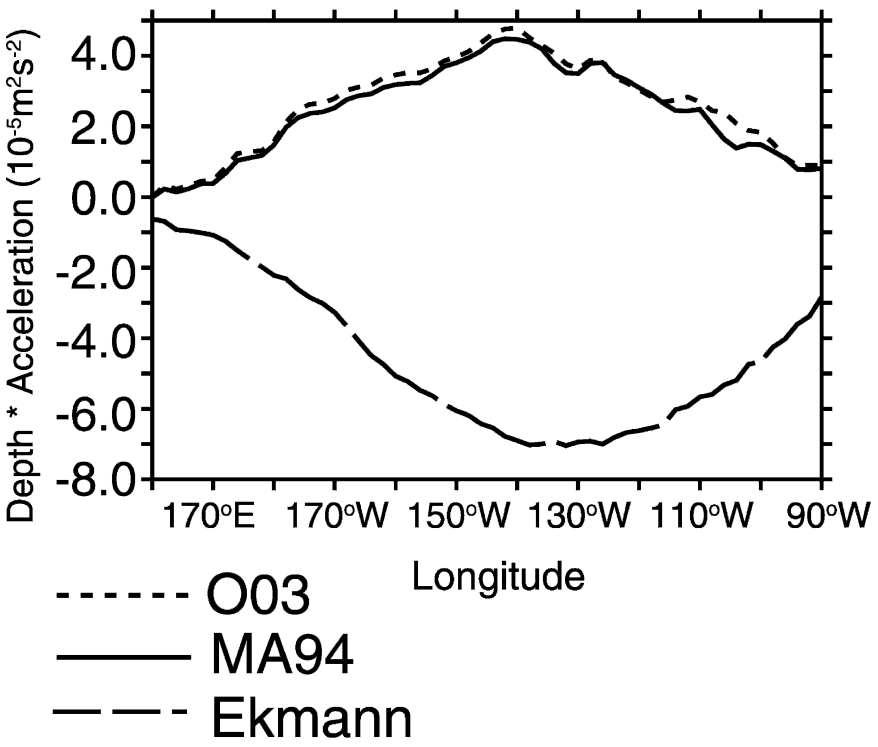

FIG. 9. Depth-integrated meridional acceleration at 5°S between 160°E and 100°W above the mixed layer. The geostrophic component of the O03 model run (short dashed line) is greater than that of the MA94 model run (solid black line). The depth-integrated meridional acceleration due to Ekman (long dashed line) is constant for both models. The sum of geostrophic and Ekman components is the total depth-integrated meridional acceleration (fM_y) above the mixed layer.

out to 10° latitude and then tapered to the O03 parameterization poleward of 15° latitude. In this case the change in overturning circulation clearly shows the predicted response: a slowdown in overturning circulation due to deeper mixed layers from ~10° poleward to 30° latitude (Fig. 12). While there is only an overturning response from ~10° to 30° latitude, small increases in temperature (0.1°C) in the thermocline at latitudes below 10° are evident (Fig. 13) indicating an increase in transport of heat below the mixed layer toward the equatorial region. The increase in transport of heat from the extratropics to the equator due to deeper solar irradiance penetration beyond latitudes of 10° is further exhibited by the reduction in restoring heat flux needed at the equator (Fig. 14).

While it clear that changing the parameterization of shortwave penetration depth using chlorophyll *a* concentrations makes a difference to the ocean circulation and heat transport, it is important to point out how changes in chlorophyll *a* concentration might change ocean circulation and heat transport. In particular, this study does not address how interseasonal or interannual variability in chlorophyll *a* concentration might affect ocean circulation or heat transport. In each model scenario the seasonal variability remains constant with no interannual variability. In addition, the differences shown between models are the result of 10-yr runs—the time necessary to reach a mechanical steady state in the tropical ocean. The results of this study illustrates how the meridional circulation and heat transport may change as a result of long term (> 1 yr), secular changes in chlorophyll *a* concentration both on and off the equator. On the equator, satellite observations of chlorophyll *a* suggest increases of almost 25% in surface chlorophyll *a* based on a comparison CZCS (1979–86) and SeaWiFS (1997–2000) records (Gregg and Conkright 2002). While these changes may be significant, it is difficult to assess how the observed trends in chlorophyll *a* have been biased by interannual variability on the equator. In particular, the SeaWiFS record does not include an El Niño event. Off the equator, at midlatitudes, satellite observations do not indicate that large changes in chlorophyll *a* have occurred in the long term. However, a time series of field measurements made in the North Pacific subtropical gyre (Karl et al. 2001; Venrick 1992, 1999; Venrick et al. 1987) show that chlorophyll *a* concentrations have more than doubled in the last three decades. A doubling of chlorophyll *a* concentrations from an average value of 0.04 mg (Chl *a*) m^{-3} to the present values 0.08 mg (Chl *a*) m^{-3} in the North Pacific subtopical gyre region would result in a 20% decrease in the penetra-

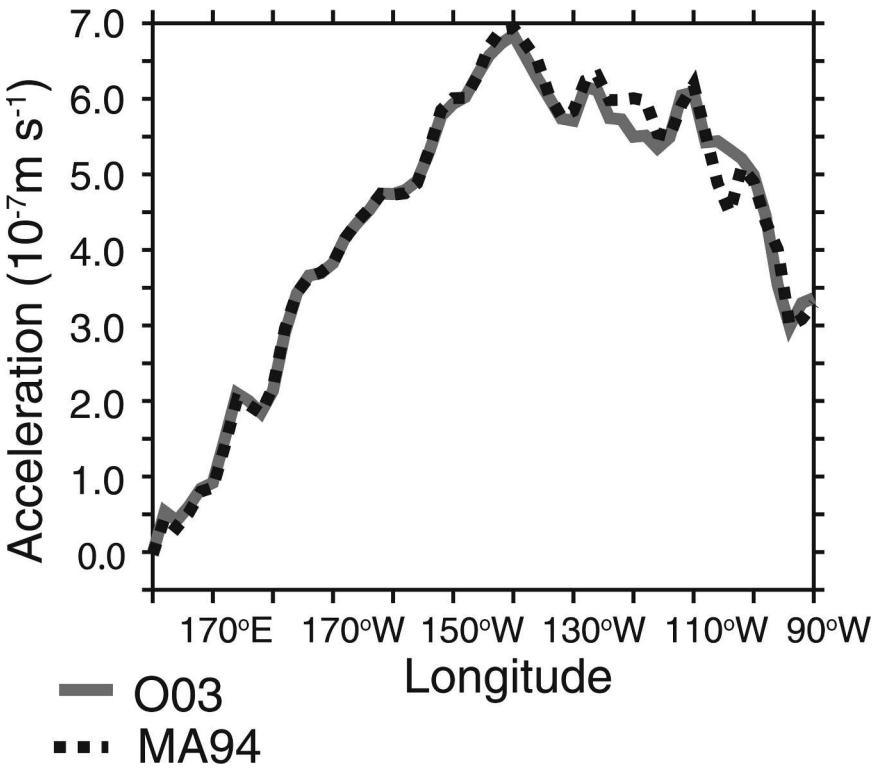

FIG. 10. The zonal pressure gradient ($\partial p/\rho\partial x$) along 5°S between model run using O03 shortwave irradiance parameterization (solid black line) and model run using MA94 shortwave irradiance parameterization (dashed line). The small difference between zonal pressure gradients in both models indicates that this does not explain the differences between meridional mass fluxes in the mixed layer.

tion depth of solar irradiance in that region. This decrease in penetration depth is almost twice the difference between the O03 and MA94 parameterization in that region. From this perspective, the relevance of comparing the O03 and MA94 parameterizations is highly justified.

Since the days of Sverdrup (1953), there has been a strong belief that the inventory of light-adsorbing biomass in the water column is strongly controlled by mixed layer depth. It is therefore hard to assert that the observations of increased chlorophyll *a* concentrations in the North Pacific subtropical gyre will drive significant changes in the mixed layer depth since both mixed layer depth and chlorophyll *a* concentration are coupled and feed back on one another. By comparing the O03 and MA94 parameterizations, we are able to explore the relative role that light penetration plays in the feedback between ocean primary productivity and ocean circulation. Based on the results of this study, we expect that increases in chlorophyll *a* concentration would result in a decreased heat transport to the Tropics below the thermocline because of a decrease in penetration depth. Concurrently, we would also expect an increase in the meridional overturning circulation in the areas where mixed layer depth decreased. Further work is needed using an OGCM with interactive biogeochemistry to understand the full extent of the coupling between chlorophyll *a* concentration and ocean circulation.

c. Relevance of simulation to other studies

The effect of changing mixed layer depth through the parameterization of solar irradiance in water on the GCM provides significant insight into the mechanisms driving other modeling results. It also provides insight into how changes in biological production may affect circulation and the air–sea exchange of heat.

As with this study, previous studies by Murtugudde et al. (2002) and Nakamoto (2001) show that while a decrease in the attenuation depth of solar irradiance in the eastern equatorial Pacific causes mixed layer depths to decrease, there is no associated increase in SST as one might conclude when using a simple one-dimensional model. Nakamoto et al. (2001) use an isopycnal ocean GCM to show that 20-m decreases in mixed layer depths in the eastern equatorial Pacific due to higher chlorophyll *a* concentrations are concurrent with 2°C decreases in SST. In a similar study, Murtugudde et al. (2002) show that mixed layer depths de-

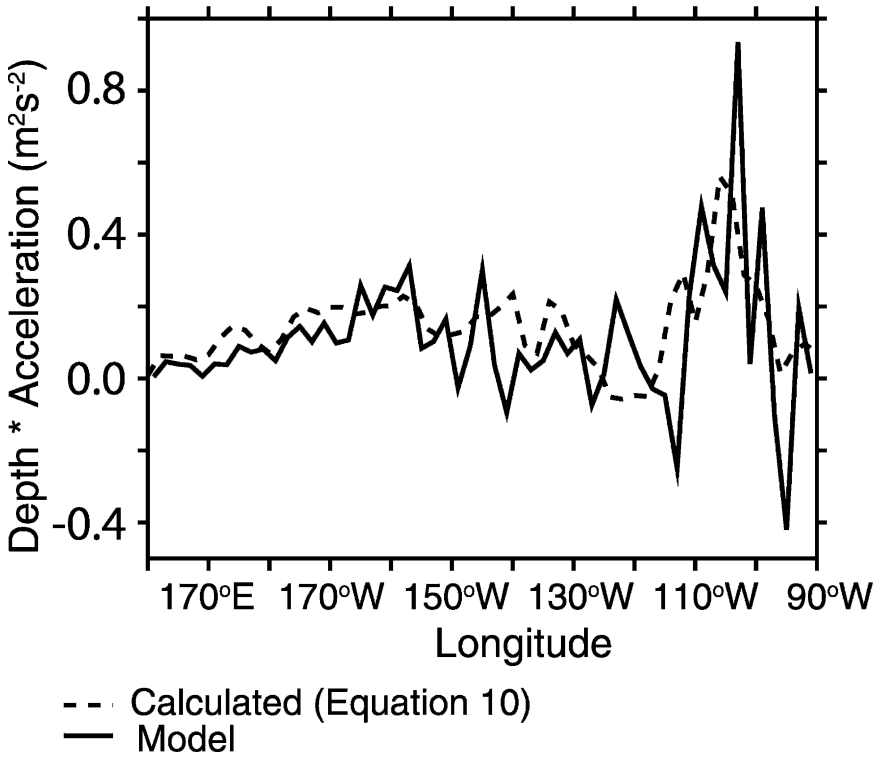

FIG. 11. The difference between the total calculated mixed layer depth integrated meridional acceleration (fM_y, dashed line) calculated from Eq. (10) using the O03 and MA94 parameterizations is compared directly with the model diagnostics (solid black line) at 5°S in the equatorial Pacific. The clear spatial similarity between calculated, and the model-simulated differences between models indicates mixed layer depths are a dominant source of the variability in meridional mass flux.

crease with increases in the attenuation of solar irradiance in the water column and that the change in SST is negative. However, Murtugudde et al. (2002) also suggest that both the response of the mixed layer depth and SSTs are variable depending on the degree to which the attenuation of solar irradiance is changed. While a change from a 25-m to 19-m shortwave attenuation *e*-folding depth in the eastern equatorial region made little difference to SSTs, a further decrease in attenuation depth to 17 m made a large difference in SST (~1°C).

Although Murtugudde et al. (2002) argue that the difference in response to changes in *e*-folding depth of solar irradiance at the equator is merely the result of absolute changes in radiant energy below the thermocline, it is also likely that changes in mixed layer depths off the equator have an impact. As noted above, Murtugudde et al. (2002) run three different scenarios: one with a constant attenuation depth of 25 m, one with a constant depth of 17 m, and one with a variable depth attenuation based on the chlorophyll *a* concentration. In the scenario with variable attenuation depths, the mean attenuation depth is 19 m in the eastern equatorial Pacific and ~25 m in the subtropical gyres. Thus, there is little difference between the penetration depths in the subtropical gyre regions when comparing the Murtugudde et al. (2002) experiment with a constant attenuation depth of 25 m to the experiment using spatially varying attenuation depths. Considering the observation made in our study, it is likely that the larger difference in equatorial SST observed by Murtugudde et al. (2002) between a spatially constant attenuation depth of 17 m and a spatially variable attenuation depth experiment is, in part, due to large differences in penetration depths off the equator.

d. Impact of off-equatorial processes on the equator

The off-equatorial impact can be demonstrated from two perspectives in this study. The first is the correlation between changes in meridional overturning circulation and off-equatorial changes in mixed layer depth demonstrated above [Eq. (10)]. With increases in mixed layer depth through deeper penetration of shortwave irradiance, there is a decrease in meridional divergence resulting in less upwelling of cold sub-mixed-layer waters. The result is a decrease in restoring heat flux, which is likely to translate into an increase in SSTs in a coupled ocean–atmospheric model. The second perspective is the longer term (>1 yr) transport of heat

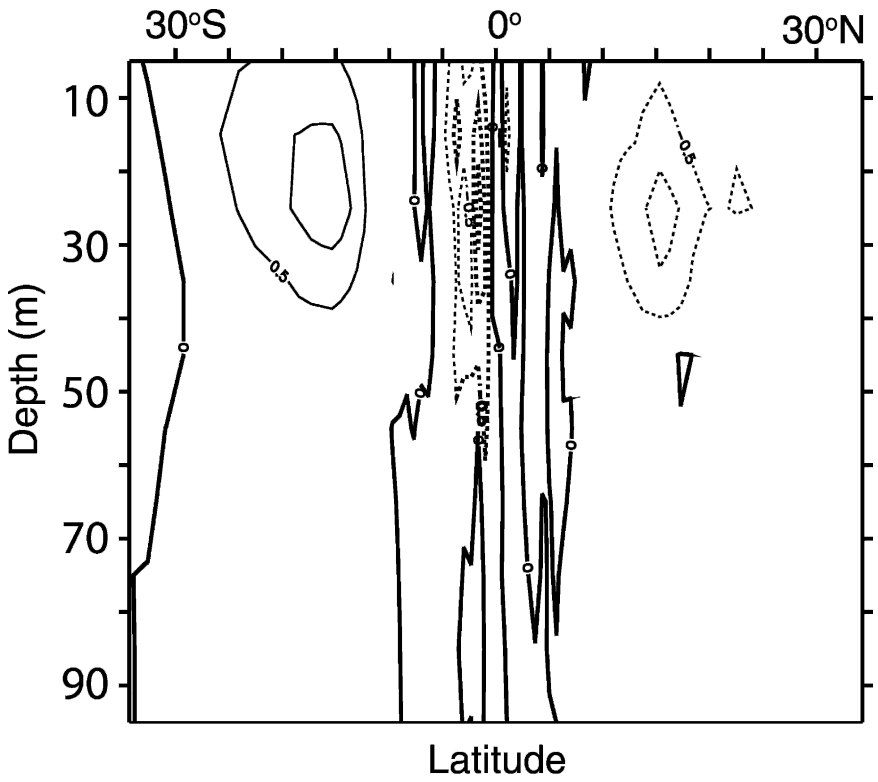

FIG. 12. Difference in the meridional overturning (Sv) from 30°S to 30°N in the Indian and Pacific Ocean basins due to a change in parameterization of solar irradiance throughout the water column at latitudes greater than 10° (O03 – MA94).

stored below the mixed layer with deeper penetration of solar irradiance in tropical and subtropical regions off the equator. This is demonstrated by the decrease in restoring heat flux at the equator resulting from moving to the deeper O03 parameterization in waters beyond 10° latitude (Fig. 14). The temperature changes in the thermocline at the equator appear to be the result of transport along isopycnals below the mixed layer from the extratropics (Fig. 13). Thus, the increase in temperatures below the mixed layer on the equator resulted in a decrease in the restoring heat flux needed to maintain SSTs at the equator (Fig. 14) despite the fact that no changes were made to the solar irradiance penetration depth at the equator. This result would imply that the deeply penetrating irradiance parameterization of O03 outside the equatorial region may be adding significant amounts of heat into the equatorial region. By inference, a decrease in chlorophyll *a* concentrations off the equatorial regions may act to increase SSTs at the equator. In summary, both deeper mixed layers off the equator and the transport of excess heat from the extratropics are mechanisms that are likely to affect SST at the equator.

This study has two important implications for our understanding of the overturning circulation and heat transport. The first is that when looking at near-equatorial dynamics, it is a mistake to think of the mixed layer as dynamically thin. In theoretical studies such as Luyten et al. (1983) the mixed layer is considered to be thin in comparison with the layers carrying the geostrophic, wind-driven flow. With such a limit, the Ekman pumping into the ventilated thermocline is essentially due to the wind stress alone. However, near the equator, the poleward flow in the mixed layer is balanced by an equatorward flow over a few hundred meters depth. A 50-m-deep mixed layer overlaps a substantial fraction of this flow. Changing the mixed layer depth induces a significant change in the Ekman pumping felt by the main thermocline.

The model results also have implications for understanding the relationship between mechanical forcing of the ocean and thermal heat transport by the ocean. The meridional overturning circulation is mechanically driven (Munk and Wunsch 1998; Toggweiler and Samuels 1998; Huang 1999; Gnanadesikan et al. 2005). For many years it has been thought that increasing mechanical mixing within the pycnocline would result in an increase in watermass conversion and poleward heat transport. An increasing flux of mechanical energy leads to an increased storage of available potential energy and thus more heat transport. However, this study demonstrates that such a relationship is not true for all energy inputs. While increasing the penetration of shortwave radiation does result in an increase in avail-

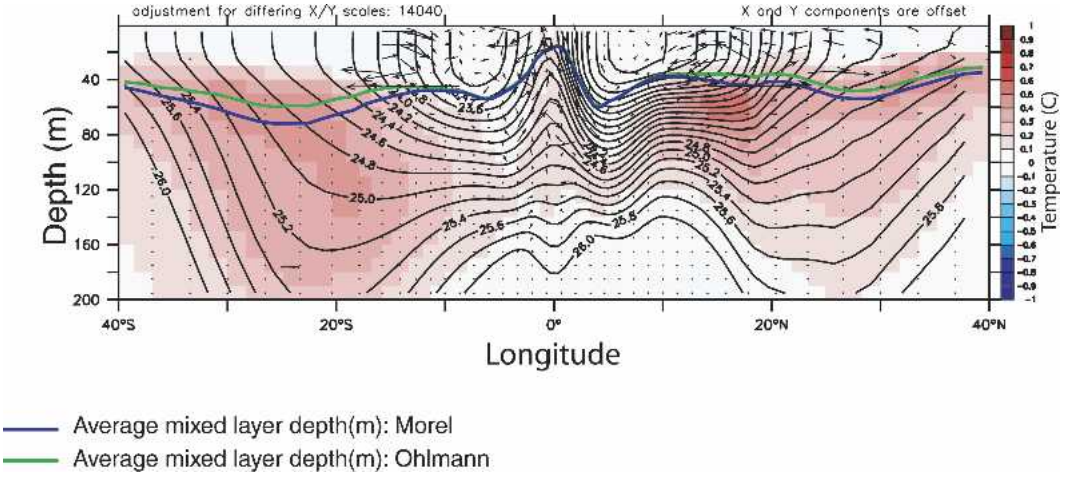

FIG. 13. Contour lines show σ_τ for MA94 line, and color indicates magnitude of temperature difference between O03 and MA94 at latitudes greater than 10°. Vector arrows signify difference in average vertical and zonal flow. Blue line indicates the average mixed layer depth for MA94, and the green line indicates the average mixed layer depth for O03. Mixed layers depths are defined in each model as the depth at which the density is 0.03 kg m^{-3} greater than the surface density.

able potential energy, as heat is stirred deeper into the water column, it is also associated with a *decrease* in heat transport and watermass conversion. Gnanadesikan et al. (2002) found a similar result when they increased mixing within the surface layer in a 4° GCM. In conclusion, one cannot extrapolate simply from mechanical energy input to heat transport.

5. Summary

A *z*-coordinate ocean GCM restored to surface temperatures and forced with climatological wind, heat, and freshwater fluxes was used to study the effects of two different surface chlorophyll *a* concentration dependent parameterizations of solar irradiance. The two different parameterizations picked in this study represent a realistic sensitivity test making it possible to quantify how large-scale ocean circulation and heat transport will be affected by different solar irradiance parameterizations and observed chlorophyll *a* concentrations.

The 1% solar irradiance depth changed between parameterizations from 10% in high–chlorophyll *a* areas (>1 mg m^{-3}) to 18% in the low–chlorophyll *a* areas (<0.05 mg m^{-3}). The model results show a concurrent increase in mixed layer depth whose magnitude was presumably determined by vertical density gradient, wind speed, light penetration depth and existing mixed layer depth. While the change in mixed layer depth above 40° latitude is not significant, the mixed layer depth increase is small (<3 m) on the equator and large (~20 m) in the subtropical gyre areas. Changes in mixed layer depth and the additional heat added to the thermocline in the extratropics result in an 8% slow-

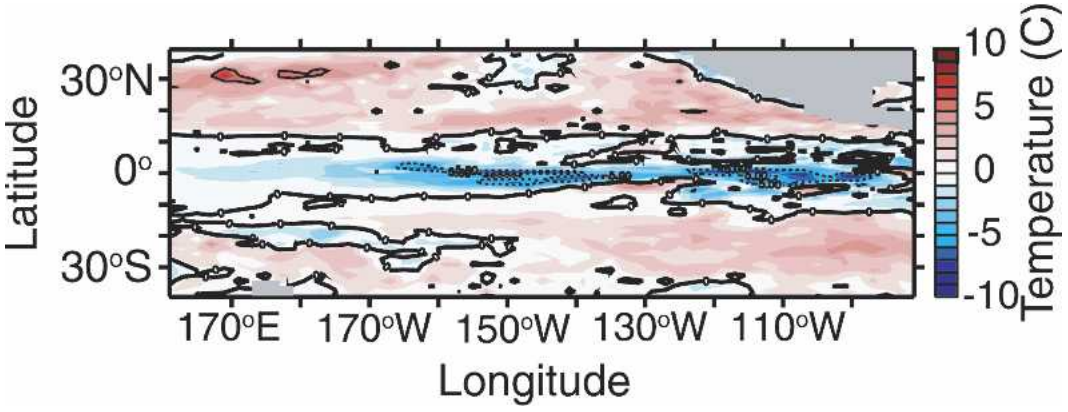

FIG. 14. Difference in restoring heat flux (W m^{-2}) as a result of different parameterization of penetrating solar irradiance at latitudes greater than 10°. Ohlmann (2003) minus Morel and Antoine (1994).

down in meridional overturning circulation. With a decrease in overturning circulation there is a slowdown in the divergence of the surface waters and 10% decrease in restoring heat fluxes needed to maintain SST at climatological values. Off the equator, increasing mixed layer depths result in an increase in restoring heat fluxes because of entrainment of deeper waters into the mixed layer

Even in the event that changes in the penetration depth are made only in the extratropics, there are significant changes to the restoring heat fluxes at the equator. This observation confirms the fact that changes in off-equatorial mixed layer depth and heat added below the thermocline contribute significantly to the surface heat content of the equatorial Pacific and Atlantic Ocean. We infer from this study that basin-scale, long-term (>1 yr) increases in chlorophyll *a* off the equator will translate into decreases SSTs at the equator. From this perspective, increases in surface water chlorophyll *a* concentration such as those observed in the North Pacific subtopical gyre region will impact meridional circulation and heat transport at the equator with lower SST. This off-equatorial effect will counteract the warming of SST due to local increases in chlorophyll a concentrations observed in the eastern equatorial regions.

Acknowledgments. This work was done with the support of the NOAA/GFDL Visiting Scientist Program and benefited from the large collaborative efforts of GFDL to build MOM4. It also benefited from the comments of two anonymous reviewers.

APPENDIX A

Constants for the Morel and Antoine Solar Irradiance Parameterization

Constants for the Morel and Antoine (1994) solar irradiance parameterization [Eq. (6)] have been estimated using the log of remotely sensed chlorophyll *a* concentration [$C = \log_{10}(\text{Chl})$, mg m^{-3}]:

$$V_1 = 0.321 + 0.008C + 0.132C^2 + 0.038C^3 - 0.017C^4 - 0.007C^5,$$

$$V_2 = 0.679\,197 - 0.008\text{C} - 0.132C^2 - 0.038C^3 + 0.017C^4 + 0.007\text{C}^5,$$

$$\zeta_1 = 1.540 - 0.166\text{C}^2 - 0.252\text{C}^3 - 0.055\text{C}^4 + 0.042\text{C}^5,$$

and

$$\zeta_2 = 7.925 - 6.644C + 3.662C^2 - 1.815C^3 - 0.218C^4 + 0.502C^5.$$

APPENDIX B

Constants for the Ohlmann (2003) Solar Irradiance Parameterization

Constants for the Ohlmann (2003) solar irradiance parameterization [Eq. (9)] have been estimated using remotely sensed chlorophyll *a* concentration (Chl, mg m^{-3}) [coefficients V_2 were suggested by J. C. Ohlmann (2003, personal communication)]:

$$V_1 = 0.571 + 0.025\ln(0.149\ \text{Chl}),$$

$$V_2 = 0.223\,740\,07 - 0.016\,093\,14\ln(2.333\,845\,54\ \text{Chl}),$$

$$\zeta_1 = 0.015 + 0.176(0.462\ \text{Chl})^{1/2}, \quad \text{and}$$

$$\zeta_2 = 0.688 + 0.060\ln(0.125\ \text{Chl}).$$

REFERENCES

Bryan, K., and L. J. Lewis, 1979: Water mass model of the World Ocean. *J. Geophys. Res.,* **84,** 2503–2517.

Denman, K. L., 1973: A time-dependent model of the upper ocean. *J. Phys. Oceanogr.,* **3,** 173–184.

Dickey, T. D., and J. J. Simpson, 1983: The influence of optical water type on the diurnal response of the upper ocean. *Tellus,* **35B,** 142–154.

Gent, P. R., J. Willebrand, T. J. McDougall, and J. C. McWilliams, 1995: Parameterizing eddy-induced tracer transports in ocean circulation models. *J. Phys. Oceanogr.,* **25,** 463–474.

Gildor, H., A. H. Sobel, M. A. Cane, and R. N. Sambrotto, 2003: A role for ocean biota in tropical intraseasonal atmospheric variability. *Geophys. Res. Lett.,* **30,** 1460, doi:10.1029/2002GL016759.

Gnanadesikan, A., R. D. Slater, N. Gruber, and J. L. Sarmiento, 2002: Oceanic vertical exchange and new production: A comparison between models and observations. *Deep-Sea Res.,* **49B,** 363–401.

——, ——, P. S. Swathi, and G. K. Vallis, 2005: The energetics of ocean heat transport. *J. Climate,* in press.

Gregg, W. W., and M. E. Conkright, 2002: Decadal changes in global ocean chlorophyll. *Geophys. Res. Lett.,* **29,** 1730–1734.

Griffies, S. M., 1998: The Gent–McWilliams skew flux. *J. Phys. Oceanogr.,* **28,** 831–841.

——, and R. W. Hallberg, 2000: Biharmonic friction with a Smagorinsky viscosity for use in large-scale eddy-permitting ocean models. *Mon. Wea. Rev.,* **128,** 2935–2946.

——, A. Gnanadesikan, R. C. Pacanowski, V. D. Larichev, J. K. Dukowicz, and R. D. Smith, 1998: Isoneutral diffusion in a *z*-coordinate ocean model. *J. Phys. Oceanogr.,* **28,** 805–830.

——, R. C. Harrison, R. C. Pacanowski, and A. Rosati, 2003: A technical guide to MOM4. GFDL Ocean Group Tech. Rep. 5, 295 pp.

Holland, W. R., J. C. Chow, and F. O. Bryan, 1998: Application of a third-order upwind scheme in the NCAR ocean model. *J. Climate,* **11,** 1487–1493.

Huang, R. X., 1999: Mixing and energetics of the oceanic thermohaline circulation. *J. Phys. Oceanogr.,* **29,** 727–746.

Jerlov, N. G., 1968: *Optical Oceanography*. Elsevier Press, 194 pp.

Karl, D. M., R. R. Bidigare, and R. M. Letelier, 2001: Long-term changes in plankton community structure and productivity in the North Pacific Subtropical Gyre: The domain shift hypothesis. *Deep-Sea Res.,* **48B,** 1449–1470.

Large, W. G., J. C. McWilliams, and S. C. Doney, 1994: Oceanic vertical mixing—A review and a model with a nonlocal boundary-layer parameterization. *Rev. Geophys.,* **32,** 363–403.

Lewis, M. R., J. J. Cullen, and T. Platt, 1983: Phytoplankton and

thermal structure in the upper ocean: Consequences of nonuniformity in chlorophyll profile. *J. Geophys. Res.,* **88C**, 2565–2570.
Luyten, J., J. Pedlosky, and H. Stommel, 1983: Climatic inferences from the ventilated thermocline. *Climate Change,* **5,** 183–191.
Martin, P. J., 1985: Simulation of the mixed layer at OWS November and Papa with several models. *J. Geophys. Res.,* **90,** 903–916.
Mobley, C. D., 1994: *Light and Water.* Academic Press, 592 pp.
Morel, A., 1988: Optical modeling of the upper ocean in relation to its biogenous matter content (case-I waters). *J. Geophys. Res.,* **93,** 10 749–10 768.
——, and J.-F. Berthon, 1989: Surface pigments, algal biomass profiles, and potential production of the euphotic layer: Relationship reinvestigated in view of remote-sensing applications. *Limnol. Oceanogr.,* **34,** 1542–1562.
——, and D. Antoine, 1994: Heating rate within the upper ocean in relation to its biooptical state. *J. Phys. Oceanogr.,* **24,** 1652–1665.
Munk, W., and C. Wunsch, 1998: Abyssal recipes II: Energetics of tidal and wind mixing. *Deep-Sea Res.,* **45A,** 1977–2010.
Murray, R. J., 1996: Explicit generation of orthogonal grids for ocean models. *J. Comput. Phys.,* **126,** 251–273.
Murtugudde, R., J. Beauchamp, C. R. McClain, M. Lewis, and A. J. Busalacchi, 2002: Effects of penetrative radiation on the upper tropical ocean circulation. *J. Climate,* **15,** 470–486.
Nakamoto, S., S. P. Kumar, J. M. Oberhuber, J. Ishizaka, K. Muneyama, and R. Frouin, 2001: Response of the equatorial Pacific to chlorophyll pigment in a mixed layer isopycnal ocean general circulation model. *Geophys. Res. Lett.,* **28,** 2021–2024.
Ohlmann, J. C., 2003: Ocean radiant heating in climate models. *J. Climate,* **16,** 1337–1351.
——, and D. A. Siegel, 2000: Ocean radiant heating. Part II: Parameterizing solar radiation transmission through the upper ocean. *J. Phys. Oceanogr.,* **30,** 1849–1865.
——, ——, and C. Gautier, 1996: Ocean mixed layer radiant heating and solar penetration: A global analysis. *J. Climate,* **9,** 2265–2280.
——, ——, and L. Washburn, 1998: Radiant heating of the western equatorial Pacific during TOGA–COARE. *J. Geophys. Res.,* **103,** 5379–5395.
Pacanowski, R. C. and S. M. Griffies, 1999: The MOM3 manual. GFDL Ocean Group Tech. Rep. 44, 680 pp.
Paulson, C. A., and J. J. Simpson, 1977: Irradiance measurements in the upper ocean. *J. Phys. Oceanogr.,* **7,** 952–956.
Redi, M. H., 1982: Oceanic isopycnal mixing by coordinate rotation. *J. Phys. Oceanogr.,* **12,** 1154–1158.
Rochford, P. A., A. B. Kara, A. J. Wallcraft, and R. A. Arnone, 2002: Importance of solar subsurface heating in ocean general circulation models. *J. Geophys. Res.,* **106,** 30 923–30 938.
Roeske, F., 2001: An atlas of surface fluxes based on the ECMWF reanalysis—A climatological dataset to force global ocean general circulation models. Max Planck-Institut fur Meteorologie Rep. 323, 31 pp.
Rosati, A., and K. Miyakoda, 1988: A general-circulation model for upper ocean simulation. *J. Phys. Oceanogr.,* **18,** 1601–1626.
Schneider, E. K., and Z. X. Zhu, 1998: Sensitivity of the simulated annual cycle of sea surface temperature in the equatorial Pacific to sunlight penetration. *J. Climate,* **11,** 1932–1950.
Siegel, D. A., T. K. Westberry, and J. C. Ohlmann, 1999: Cloud color and ocean radiant heating. *J. Climate,* **12,** 1101–1116.
——, J. C. Ohlmann, L. Washburn, R. R. Bidigare, C. T. Nosse, E. Fields, and Y. Zhou, 1995: Solar radiation, phytoplankton pigments and the radiant heating of the equatorial Pacific warm pool. *J. Geophys. Res.,* **100,** 4885–4891.
Simpson, J. J., and T. D. Dickey, 1981: Alternative parameterizations of downward irradiance and their dynamical significance. *J. Phys. Oceanogr.,* **11,** 876–882.
Smagorinsky, J., 1963: General circulation experiments with the primitive equations. Part I: The basic experiment. *Mon. Wea. Rev.,* **91,** 99–164.
Strutton, P. G. and F. P. Chavez, 2004: Biological heating in the equatorial Pacific: Observed variability and potential for real-time calculation. *J. Climate,* **17,** 1097–1109.
Sverdrup, H. U., 1953: On conditions for the vernal blooming of phytoplankton. *J. Conseil,* **18,** 287–295.
Toggweiler, J. R., and B. Samuels, 1998: On the ocean's large-scale circulation near the limit of no vertical mixing. *J. Phys. Oceanogr.,* **28,** 1832–1852.
Venrick, E. L., 1992: Phytoplankton species structure in the central North Pacific—Is the edge like the center. *J. Plankton Res.,* **14,** 665–680.
——, 1999: Phytoplankton species structure in the central North Pacific, 1973–1996: Variability and persistence. *J. Plankton Res.,* **21,** 1029–1042.
——, J. A. McGowan, D. R. Cayan, and T. L. Hayward, 1987: Climate and chlorophyll-a—Long-term trends in the central North Pacific Ocean. *Science,* **238,** 70–72.
Woods, J. D., and R. Onken, 1982: Diurnal variation and primary production in the ocean—Preliminary results of a Lagrangian ensemble model. *J. Plankton Res.,* **4,** 735–756.
——, W. Barkmann, and A. Horch, 1984: Solar heating of the oceans—Diurnal, seasonal and meridional variation. *Quart. J. Roy. Meteor. Soc.,* **110,** 633–656.
Yoder, J. A., and M. A. Kennelly, 2003: Seasonal and ENSO variability in global ocean phytoplankton chlorophyll derived from 4 years of SeaWiFS measurements. *Biochem. Cycles,* **17** (4), 1112, doi:10.1029/2002GB001942.